JOURNAL OF PROPULSION AND POWER
Vol. 19, No. 2, March–April 2003

Vortex Shedding Induced Sound Inside a Cold-Flow Simulation of Segmented Chamber

Alison Flatau*
University of Maryland, College Park, Maryland 2074
and
W. K. Van Moorhem†
University of Utah, Salt Lake City, Utah 84112-9208

Results are presented from a cold-flow investigation of acoustic responses driven by flow through two annular baffles in a cylindrical cavity, having (approximately) closed–closed end conditions. The interaction of the flow with cavity acoustic resonances was examined for different baffle radii, positions, spacings, and stiffness. Nominal vortex shedding frequencies were found to depend on baffle spacing and radii (flow velocity), with little sensitivity to baffle stiffness. Vortex shedding lock-in frequencies were very sensitive to acoustic pressures and/or acoustic particle velocities acting on the flow at both the upstream and downstream baffles. Vortex shedding lock-in occurred in conjunction with acoustic standing waves formed between the baffles and ends of the test chamber such that either acoustic pressure maxima (closed conditions) occurred at the upstream baffle or acoustic velocity maxima (pressure release or open conditions) occurred at the downstream baffle. High acoustic pressure at the upstream baffle appeared to enhance the strength of the shed vortices, and low acoustic pressure (high acoustic particle velocity) at the downstream baffle appeared to enhance the strength of the acoustic field radiated on vortex impingement. For most of the two baffle geometries, baffle-to-nozzle acoustic modes were the dominant mechanism responsible for lock-in and strong reinforcement of vortex shedding driven acoustic excitation.

Introduction

A NUMBER of large solid-propellant rocket motors, including the space shuttle, Titan, and Ariane 5 solid boosters, exhibit instabilities due to vortex shedding driven acoustic pressure oscillations. There are two mechanisms believed to drive the formation of these vortices. The first is flow past protrusions into the flowfield at chamber segment interfaces[1–18] (also discussed in B. Husseys 1985 internal report, "Pressure Oscillations in Recent Space Shuttle SRM Static Test Motors," Thiokol Corporation Support Services). The second is parietal or surface vortex shedding resulting from the natural instabilities in the radial flow introduced during propellant combustion.[19–26] This work reports on a cold-flow simulation of the first of these two mechanisms.

Flow through the inhibitor stubs at motor joint locations is believed to generate acoustic responses known as "hole-tone" responses, so named because of the system geometry[27–29] (also discussed in D. Rockwell's 1987 short course notes, "Flow-Induced Oscillations," at Lehigh University in Bethlehem, Pennsylvania). Several researchers[27–31] (also Rockwell, Lehigh University) present quite detailed analyses of the hole-tone generation process. Hole tones are produced when jet flow instabilities that develop into shed vortices are amplified by acoustic feedback generated as the shed flow impinges downstream on a concentric annular surface or "hole." This downstream hole or flow obstruction is the location of dipole radiation of sound that propagates in both the upstream and downstream directions in the cavity[28,29] (also Rockwell, Lehigh University). In large segmented rocket motors, the extent of protrusion into the flowfield of the different annular inhibitors at segment joints varies with time. Vortices shed from an inhibitor excite hole tones when the geometry, speed of sound in the chamber, and vortex propagation speeds are such that a self-sustaining acoustic feedback mechanism is introduced that reinforces vortex shedding. This occurs when timing and spacing are such that shed vortices impinging on either a downstream inhibitor, or the aft motor surface at the nozzle, produce pressure pulses that propagate upstream and reinforce separation of flow and shedding of even stronger vortices from the upstream inhibitor.

Several researchers have indicated that the periodicity of vortex shedding and the resultant hole tone coincide with different acoustic resonant frequencies as geometries and flow velocities vary during motor combustion.[2,5–7] One of the earlier experimental investigations of this phenomenon[6] identified inhibitor or baffle locations relative to nodes of combustion cavity axial acoustic modes as an important factor in producing hole-tone responses. These researchers observed that acoustic responses for a given configuration (baffle spacing and flow velocity) favor vortex shedding at chamber-length acoustic mode frequencies. Their findings indicate that amplified pressures occur when two closely spaced baffles are located at standing wave pressure nodes (velocity antinodes), whereas no acoustic pressure amplification results when the baffle pair is located at pressure antinodes. The current work expands on their investigation by allowing distinctions to be made between the effects of upstream and downstream baffle locations relative to the multiple resonant acoustic fields within the test chamber, with the experimental facility depicted schematically in Fig. 1.

Frequency predictions for hole tones can be made using the nondimensional Strouhal number Sr_i, the mean instability flow velocity U, and the spatial dimension d, using

$$f = Sr_i U/d \tag{1}$$

where d is defined as the distance between the surface from which the vortex is shed and the downstream impingement surface and the Strouhal number's subscript i corresponds to the integer number of flow instability oscillations that form in the span d through which the instability travels. Each Strouhal number corresponds to an integer "stage" of the oscillation, where the stage numbers i have been

Received 4 January 2002; revision received 6 November 2002; accepted for publication 11 November 2002.

*Associate Professor, Aerospace Engineering, 3181 Martin Hall. Senior Member AIAA.

†Professor, Department of Mechanical Engineering, 50 South Central Campus Drive, Room 2202. Senior Member AIAA.

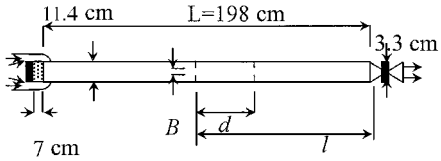

Fig. 1 Schematic of experimental facility.

compared to the number of vortices that fit in the space between the upstream and downstream surfaces.[16,32] Experimental flow visualization results presented by Nomoto and Culick[33] illustrate the presence of these stages or integral number of vortices between protrusions in a flowfield during hole-tone excitation.

Although to date no analytical approaches for determining Strouhal numbers have been identified, empirical work has identified different models and values for Strouhal numbers that are associated with a broad variety of flow, geometric, and Reynolds number interactions.[16,18,32] For instance, building on work by Rossiter,[32] Dotson et al.,[16] define the Strouhal number for this geometric configuration as

$$Sr_i = fL/U = (i - \alpha)/(M + 1/k) \tag{2}$$

with M the Mach number, i the stage number, α a dimensionless empirical constant, and k the portion of the freestream velocity at which the vorticies travel (two-thirds in Ref. 32 and 0.5–0.6 in ramjet and cavity studies sited by Dotson et al.[16]). Stubos et al.[18] contribute further related work, suggesting that variation in the propagation speed of vortices is related to baffle dimensions and demonstrating a linear correlation of the ratio of baffle to chamber diameters to the hole-tone frequency.

A "locking-in" condition occurs when structural and/or acoustic frequencies alter vortex shedding frequencies from those expected based on Eq. (1). Chanaud and Powell[28] reported that hole-tone reinforcement occurs in the presence of a downstream reflector, such as could be provided by the downstream choked-flow nozzle termination of the acoustic cavity in a rocket motor. They found that this reinforcement occurs when an odd number of hole-tone frequency one-quarter wavelengths fits in the distance between the hole that the shed vortices impinge on and a downstream reflector. Blake[29] noted that participation of a resonator (such as the acoustic modes cited by Chanaud and Powell[28]) is generally required for self-sustaining tone generation at Reynolds numbers above $\sim 3 \times 10^3$ and that variations in Reynolds numbers above this value have little effect on tone generation.

Umeda et al.[34] found that hole-tone generation from the interaction of high-speed jets and a circular hole does not occur below a minimum dimensionless spacing d/B of two, where d is the spacing between upstream and downstream baffles and B is the upstream baffle's inner diameter. On the other hand, Blake[29] presented a table suggesting that this minimum ratio is between one and two. Rockwell (Lehigh University short course notes) discussed that as the baffle spacing d increases, both the vortex strength and the acoustic disturbance strength diminish, which, respectively, results in reductions in both the induced acoustic disturbance and the vortex strength. Stubos et al.[18] show vortex shedding lock-in over a d/B range from 0.55 to 5.5, with maximum pressure amplitudes generated for $d/B = 1.2$. Thus, lower and upper bounds seem to exist on the dimensionless baffle spacing d/B for which hole-tone generation will occur.

Acoustic boundary conditions that introduce a sufficient impedance change for the generation of acoustic reflections can be modeled as either closed C or open O acoustic boundary conditions, corresponding to the impedance changes found in either rigid or pressure release boundaries, respectively. It is common practice to model combustion cavity head end and nozzle surfaces as high-impedance or closed acoustic boundary conditions (corresponding to zero velocity). Baffles have typically been modeled as open acoustic boundary conditions.

This study uses a choked-flow wind-tunnel facility to simulate the acoustic and axial flowfields in a combustion cavity. It also provides an investigation of hole-tone interaction with acoustic resonances in the following six cavities: 1) inlet to nozzle, 2) upstream baffle to nozzle, 3) downstream baffle to nozzle, 4) upstream baffle to inlet, 5) downstream baffle to inlet, and 6) upstream baffle to downstream baffle. By the use of the speed of sound in the fluid a and the cavity length of interest L in the equations for acoustic resonance of C–C and O–C cavities, potential lock-in frequencies can be predicted by classical solutions for acoustic cavities:

$$f_{\text{C–C}} = na/2L \tag{3}$$

$$f_{\text{O–C}} = (2n - 1)a/4L \tag{4}$$

where n indicates the acoustic mode number (an integer ≥ 1). The mean gas flow velocities used to produce vortex shedding were small compared with the speed of sound and were neglected.

Experimental Approach

Flow past two solid-rocket motor inhibitors was modeled in a cold-flow, choked-flow, cylindrical wind-tunnel test section.[35] Similitude of the experiment to geometries encountered in the NASA shuttle solid-rocket motors was achieved by matching dimensionless baffle spacings d/B and Mach number regimes. Shuttle Reynolds numbers are of the order 10^6, and, in this study, Reynolds numbers were on the order of 10^5. In both cases Reynolds numbers are greater than the value of $\sim 3 \times 10^3$, above which it is reported in Refs. 29 and 34 that jet tones or hole tones require the participation of an acoustic resonator. Geometric scaling factors of approximately 20–40 were applied to scale the inhibitor dimensions and spacing for different times during solid-rocket motor combustion. The test section as operated provided Reynolds numbers based on flow area diameter from 0.3 to 1.5×10^5 and Mach numbers of between 0.05 and 0.23. The test-section length was longer than the scaled motor length, providing lock-in with different acoustic cavity resonant modes in the simulation than would occur in a full-scale motor.

The experimental facility used for this research was a blowdown supersonic wind tunnel, with its test-section geometry as depicted in Fig. 1. The test section was built from a 1.98-m-long, 11.4-cm-diam thin-walled aluminum cylinder with a wall thickness of 0.7 mm. The upstream end of the test section was a solid 18-mm-thick aluminum disk. The downstream end of the test section was an 18-mm-thick aluminum disk with a 33.0-mm-diam convergent orifice that choked the flow at the end of the test section. The ends of the test section were designed to provide high-impedance acoustic termination surfaces (similar to a closed end) to support C–C inlet-to-nozzle longitudinal acoustic modes. Airflow into the test section was introduced radially through a 7.0-cm-long cylindrical porous segment of the test section adjacent to the solid upstream surface.

The wind tunnel was operated to maintain a pressure of 168 ± 14 kPa (12 ± 1 psig) in the test section. Airflow into the test section had an average inlet velocity of 28.6 m/s. The mean velocity in the 11.4-cm-diam test section was 16.4 m/s. The speed of sound in the test section was approximately 333 m/s.

Bruel & Kjær model 4138 $\frac{1}{8}$-in. microphones were used to measure the test-section acoustic pressures. One microphone, located near the test-section inlet (22 cm from the upstream surface), was used to obtain test-section pressure autospectra as baffles and baffle positions were varied. A second roving microphone was used with the first in cross-correlation functions for measurement of standing wave pressure profiles and for a separate study of the pressure between the baffles.[35] Averaged pressure autospectra and cross-correlation functions from 0–1.0 and 0–2.5 kHz were obtained using a Hewlett Packard 3582 spectrum analyzer. Data sets of 100–250 averaged spectra were obtained during 5 min of stationary steady-state flow conditions in the test section for each baffle pair position. Spectra and sound pressure levels (SPLs) are presented as measured, with decibel SPLs referenced to 20×10^{-6} Pa.

Measured acoustic standing wave mode shapes provided verification that the experimental facility approximated C–C boundary conditions.[35] Resonant acoustic standing wave mode shapes consistently exhibited pressure maxima at the downstream end of the test section, as one should find with a closed boundary condition. Mode shapes exhibited magnitudes of slightly below maxima at the

upstream end of the test section, suggesting that the radial flowfield at the upstream end of the test section introduced acoustic losses, though it did not significantly weaken the validity of an assumption of C–C boundary conditions in the test section.

Peak SPLs would ideally have been measured with a microphone positioned at a pressure antinode of an excited frequency by locating a microphone adjacent to the upstream or downstream test-section boundaries or by repositioning of the microphone. These options could not be achieved with the test setup because roughly 12 cm of the upstream portion of the test section was recessed into the airflow supply pipes, as shown in Fig. 1. The microphone position of 22 cm from the reflector at the upstream end of the test section was used because this location was believed to introduce less than a 3.5-dB error in the magnitude of SPLs over the predominant hole-tones excitation range of 600–900 Hz, where hole-tone SPLs were typically in the range of 140–150 dB. A background SPL due to flow noise was approximately 125 dB.

The SPL error estimate is based on using the assumption of having high-impedance boundary conditions (in agreement with measured test-section mode shapes) to assume the presence of cosinusoidal acoustic waveforms in the test section. The microphone position of 22 cm from the upstream boundary coincided with a pressure antinode of the test section's eighth acoustic resonant mode at 672 Hz; thus, microphone measurements detected the peak SPL in the test section at that frequency. At 756 Hz, the mode-9 pressure antinode closest to the microphone location occurred at 20 cm. As measured at 22 cm, the SPL at 756 Hz was 0.4 dB, or 5% lower than the peak level that would have been measured at the antinode. Similarly, SPL measurements were lowered by 3.4, 1.0, and 2.3 dB for modes 6, 7, and 10 at 504, 588, and 840 Hz, respectively (corresponding to pressure antinodes at 30, 26, and 18 cm). The frequencies with pressure nodes closer than antinodes to the microphone were the 12th mode at 1000 Hz and the fourth mode at 330 Hz. As measured at 22 cm from the upstream boundary, SPLs at these frequencies would be lowered by 19 and 29 dB, respectively, based on this analysis.

Initial tests were conducted using pairs of 3.175-mm-thick aluminum baffles with inner diameters B of 5.3, 5.8, or 6.3 cm. These baffles had structural resonant frequencies above 4000 Hz. The baffle inner circumference was a free surface with the inner edge cut normal to the plane of the baffle (square corners). Fixtures that moved independently along the test section held the baffles and provided a clamped outer diameter boundary condition at 8.9 cm. The baffle-to-baffle separation distance d beyond which hole tones were insufficiently reinforced to be detectable above the background acoustic level varied with each test case, but never exceeded 50 cm. The combinations of baffle inner diameters and baffle spacings tested corresponded to nondimensional baffle separations d/B of from ~1 to 8, covering the range suggested in the literature for the occurrence of hole-tone acoustic excitation.

Baffle positions are presented using the distance from the upstream baffle to the nozzle l divided by the test section length L. L was 198.0 cm in all tests. Tests were conducted at nondimensional upstream baffle positions l/L of from 0.03 to 0.88 (corresponding to 5.5–174.0 cm from the nozzle).

The influence of baffle stiffness on the hole tones was examined using baffle materials selected to appear soft and stiff in contrast with the rigid baffles described earlier. The soft baffles were made of 1.587-mm-thick rubber with their first resonant modes at approximately 380 Hz. The rubber's material properties were selected to simulate elastic properties of the nitrile butadiene rubber inhibitors used in the space shuttle motors. The stiff baffles were made of 0.203-mm-thick brass, with their first resonant mode at approximately 520 Hz. This thickness was selected so that the first few bending resonant frequencies of the baffles would overlap the range of dominant vortex shedding frequencies. Stiff baffle tests were also conducted using 0.406-mm-thick brass baffles with a first resonant mode at 700 Hz. Their second mode was at 840 Hz, that is, coincident with the 10th axial acoustic mode of the test section. (The first four resonant frequencies for the soft and stiff baffles were measured in the mounting fixtures used in the test section before and after the test and are given in Ref. 35.) Strain gauges were installed on all baffle materials; however, only the rubber and brass baffles exhibited responses above the system noise floor at frequencies below 2500 Hz. Hole-tone and baffle strain data are presented from tests using these more compliant baffles.

The last test presented reports on hole tones generated by flow past a single baffle as the flow impinged on the aft end of the test section in lieu of a downstream baffle. In this case, d and l are both equal to the distance between the sole baffle and the nozzle.

Results and Discussion

Test-Section Characterization

The background acoustic field in the test section was measured for flow in the test section without the baffle mounting fixtures and with the fixtures but no baffles. In both cases, the flow noise was broadband at SPLs of less than 125 dB. Slight increases in acoustic pressure (~1–2 dB) were measured just above the noise floor at the test-section (inlet-to-nozzle) fundamental C–C acoustic mode frequency of 84 Hz and at several higher harmonics.

In what follows, a discussion of experimental results has been organized around five test cases for evaluation of the effects of varied baffle spacing, position, diameter, and stiffness. The five test cases (and relevant Figs. 2–10) are summarized in Table 1.

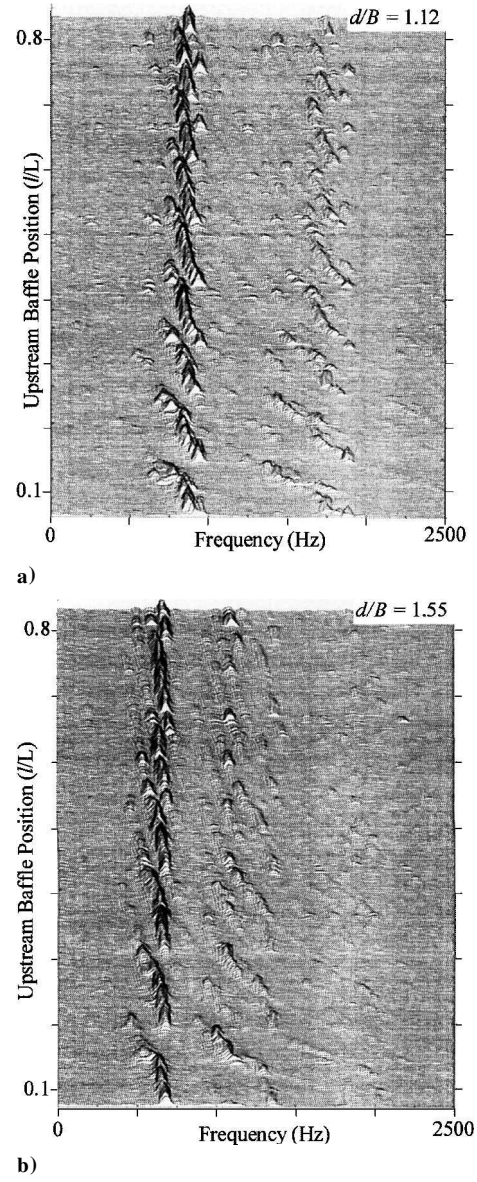

Fig. 2 Pressure autospectra for rigid baffles with baffle spacing d/B of a) 1.12 and b) 1.55 as the upstream baffle position moved from $0.1 \le l/L \le 0.9$ in 0.5-cm increments.

Table 1 Summary of test cases presented

Test case	Related Figs.	Baffle–baffle separation d	Baffle diameter B	Upstream baffle position l/L	Downstream baffle position $(l-d)/L$	Baffle stiffness
1	2–4	Fixed	Fixed	Varied	Varied	Fixed
2	5	Varied	Fixed	Fixed	Varied	Fixed
3	6	Varied	Varied	Fixed	Varied	Fixed
4	7–9	Varied	Fixed	Fixed	Varied	Varied
5	10	Varied*	Fixed	Varied	None	Fixed

*Baffle-to-nozzle separation because only one baffle used.

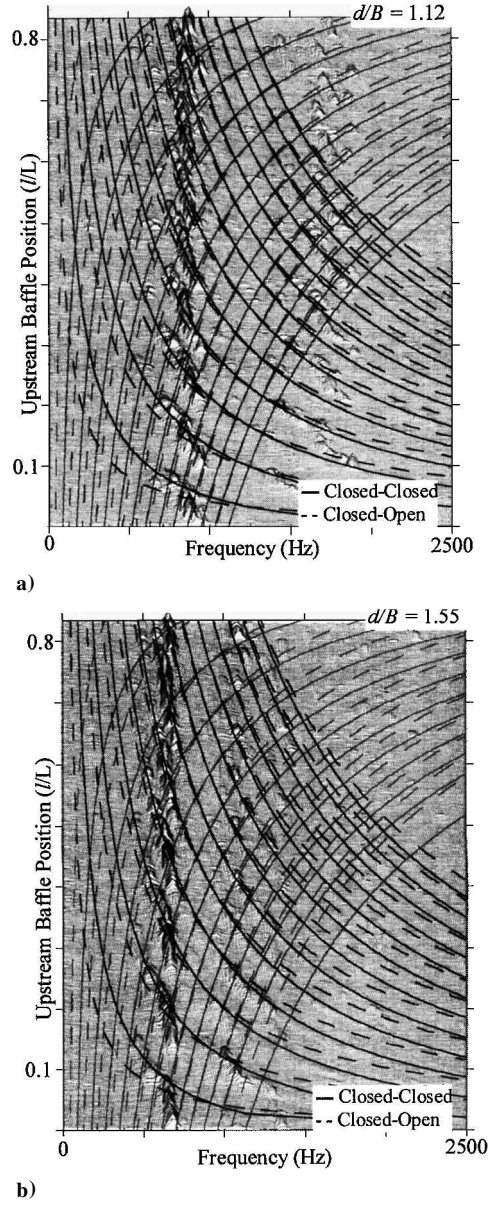

Fig. 3 Resonant frequencies in the cavities formed between baffles and ends of test section as l/L was varied for baffle spacing d/B of a) 1.12 and b) 1.55 superimposed on Fig. 2 pressure autospectra; lighter (darker) lines used for frequencies of baffle-to-inlet (-nozzle) resonance.

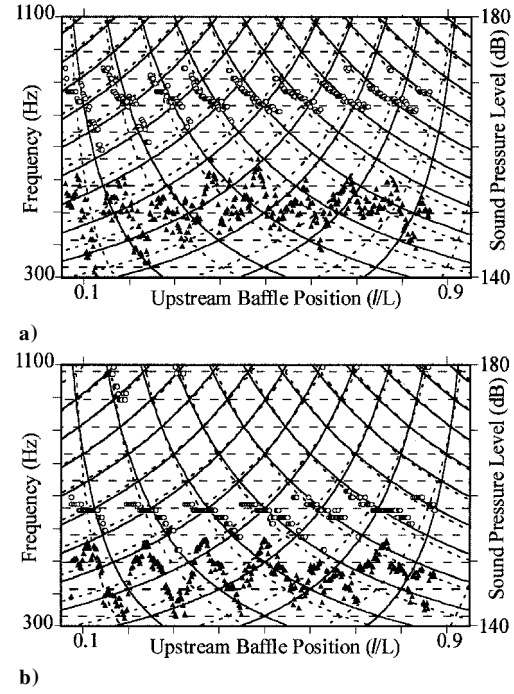

Fig. 4 Frequency and SPL corresponding to the largest acoustic response at each Fig. 2 upstream baffle position for baffle spacings d/B of a) 1.12 and b) 1.55: - - - -, downstream baffle to nozzle and inlet; ——, upstream baffle to nozzle and inlet; – – –, nozzle to inlet; ○, frequency of peak response; and ▲, SPL of peak response.

Test Case 1: Varied Baffle Pair Location (d/B = 1.12 and 1.55 and $0.07 \le l/L \le 0.87$)

Two baffles having a fixed separation d were moved along the test section to examine the influence of the acoustic resonance of different baffle-to-nozzle and baffle-to-inlet cavity lengths on vortex shedding lock-in frequency and amplitude. Pressure autospectra are presented in Figs. 2a and 2b for dimensionless baffle spacings of 1.12 and 1.55 (fixed baffle-to-baffle spacings d of 6.5 and 9.0 cm, respectively, and baffle inner diameters B of 5.8 cm). The dimensionless upstream baffle position l/L was varied from near 0.1 to 0.9 in 320 equal increments (~10–170 cm in 0.5-cm increments).

The most prominent features in Figs. 2a and 2b are the bands of vortex shedding driven hole-tones that occurred about mean frequencies of 850 and 650 Hz, respectively. Equation (1) was used to determine empirically Strouhal numbers of $Sr_1 \approx 0.86$ for the 6.5-cm data and $Sr_1 \approx 0.93$ for the 9.0-cm data, both with variability of +10 and −20%. The subscript on the Strouhal number denotes the assumption of stage-1 vortex shedding at these frequencies, that is, formation of one vortex between the baffles[3,32] (also discussed by Rockwell, Lehigh University). A second band of hole tones is apparent in the spectra at a mean frequency of 1580 Hz in Fig. 2a and at 1120 Hz in Fig. 2b. A Strouhal number of $Sr_2 \approx 1.6 \pm 10\%$ for stage-2 vortex shedding was determined for both data sets.

A second trend evident in both Figs. 2a and 2b is that the measured acoustic autospectra combine to form multiple curved ridges sweeping (convex downward) from lower frequencies at larger baffle-to-nozzle distances to higher frequencies at smaller baffle-to-nozzle distances. When these curving features intersect frequency bands of stage-1 and stage-2 vortex shedding, amplitudes of the acoustic responses increase. A third trend, producing even fainter features, most evident in the upper right of Fig. 2b (1750–2500 Hz, $l/L = 0.5$–0.8), suggests additional curved ridges sweeping (concave downward) from higher frequencies at larger baffle-to-nozzle distances to lower frequencies at smaller baffle-to-nozzle distances. Finally, as in the background flow noise measurements, minor responses detectable just above the noise floor at the test-section fundamental

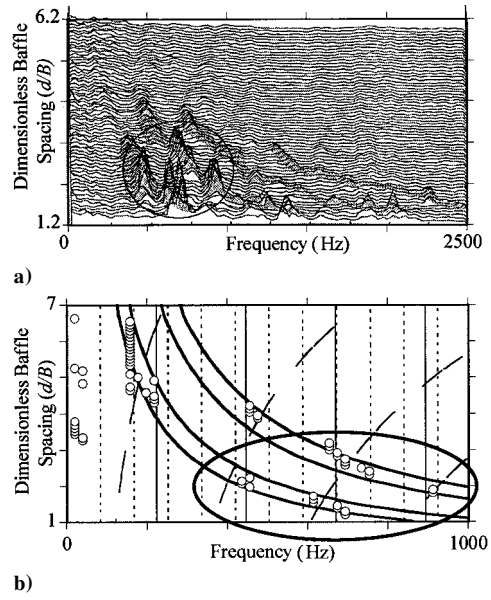

Fig. 5 Rigid baffles with spacing d/B varied from 1.2 to 6.2 and upstream baffle position fixed at $l/L = 0.37$: a) pressure spectra with shading on bands of stage 1–4 vortex shedding and b) frequencies of the largest acoustic response for each baffle spacing d/B with acoustic cavity frequencies and bands of predicted vortex shedding frequencies ($Sr_1 = 0.9 \pm 0.1$ and $Sr_2 = 1.6 \pm 0.15$) circled regions highlight jumping between stage-1 and stage-2 vortex shedding: - - - -, inlet to nozzle; – —, downstream baffle to nozzle; ——, upstream baffle to nozzle; ▬▬, Strouhal number = 0.8, 1.0, 1.5, and 1.8; and ○, frequencies of peak response.

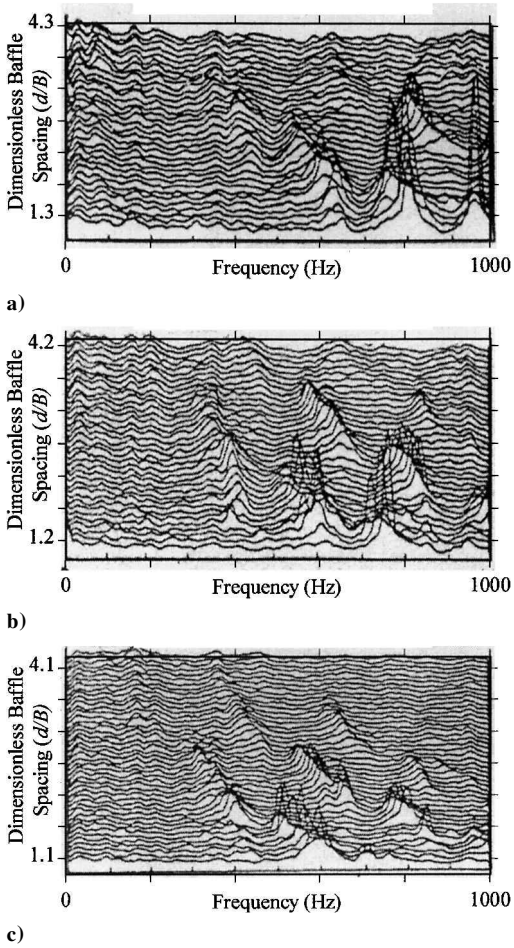

Fig. 6 Pressure autospectra for rigid baffles with inner diameters of a) 5.3, b) 5.8, and c) 6.3 cm; upstream baffle position fixed at $l/L = 0.43$.

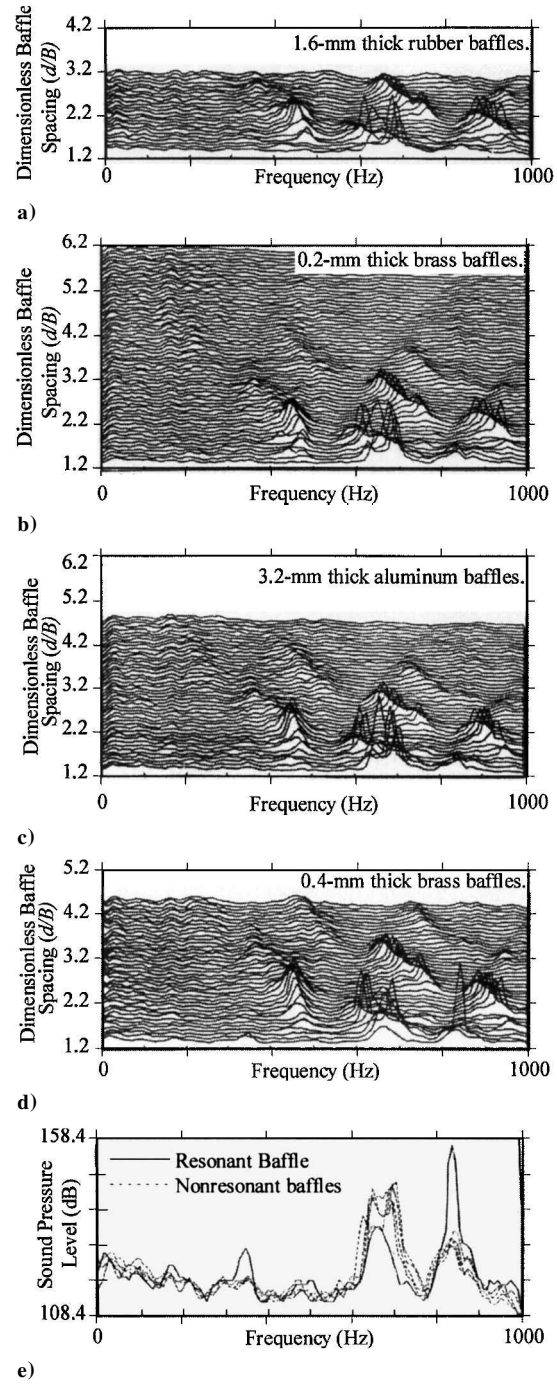

Fig. 7 Pressure autospectra for upstream baffle position $l/L = 0.38$ and for 5.8-cm-diam baffles made from a) 1.6-mm-thick rubber (soft), b) 0.2-mm-thick brass (stiff), c) 3.2-mm-thick aluminum (rigid), d) 0.4-mm-thick brass (resonant), and e) spectra from different baffle materials superimposed for baffle spacing of $d/B = 1.2$.

C–C acoustic mode, 84 Hz, and several higher harmonics are present in Figs. 2a and 2b.

In Figs. 3a and 3b, curves of the resonant acoustic frequencies [based on Eqs. (3) and (4)] that can form between the baffles and the ends of the test section have been superimposed on the data from Figs. 2a and 2b, respectively. All combinations of closed and open acoustic boundary conditions were considered for the two baffles. Closed boundary conditions were used to model the inlet and nozzle. Use of a closed boundary condition at the upstream baffle and an open or pressure release boundary condition at the downstream baffle provides an almost perfect fit to the convex downward features in Figs. 2a and 2b (the second trend cited earlier). Coincidence of curves corresponding to baffle to inlet match the fainter concave

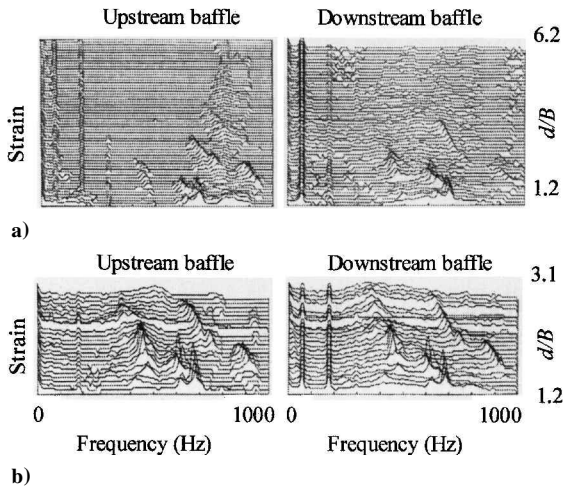

Fig. 8 Strains measured in the upstream and downstream baffles from the a) stiff (0.2-mm-thick brass) and b) soft (1.6-mm-thick) baffles; baffle diameter was $B = 5.8$ cm and upstream baffle position was $l/L = 0.38$.

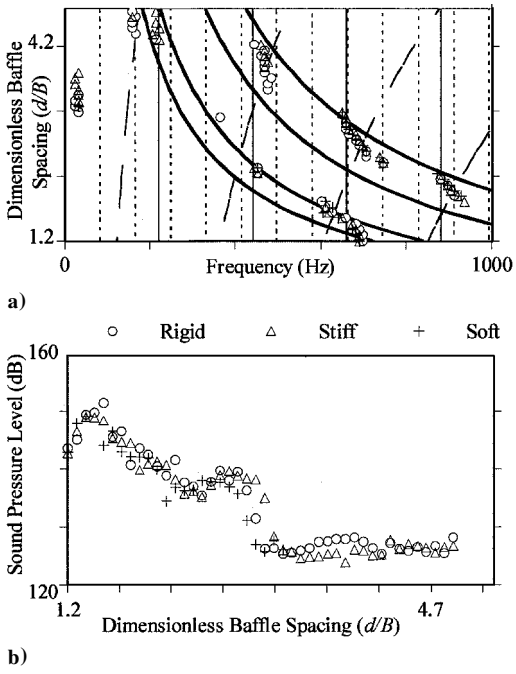

Fig. 9 Comparisons of a) frequencies and b) SPLs of the largest acoustic responses for rigid, stiff, and soft baffle materials with 5.8-cm-diam baffles and upstream baffle position $l/L = 0.38$: - - - -, inlet to nozzle; – —, downstream baffle to nozzle; ——, upstream baffle to nozzle; ——, Strouhal number = 0.8, 1.0, 1.5, and 1.9; and ○, rigid; △, stiff; and +, soft.

downward features at larger l/L and higher frequencies (the third trend cited earlier) and fills in the region of $l/L < 0.3$ where resonance of the baffle-to-nozzle cavities had failed to coincide with hole-tone peaks in the spectra.

These curves suggest that a good approximation to the acoustic impedance at the baffles is achieved by modeling the upstream baffle as a closed acoustic boundary and by modeling the downstream baffle as an open acoustic boundary. This model for the downstream baffle agrees with Chanaud and Powell's observation that hole-tone reinforcement occurs when an odd number of hole-tone frequency one-quarter wavelengths fit in the distance between the hole (the downstream baffle) and a downstream reflector (the nozzle end of the test section).[28] For the two-baffle studies presented, upstream baffle-to-inlet and upstream baffle-to-nozzle cavities are modeled as C–C cavities, and downstream baffle-to-inlet and downstream baffle-to-nozzle cavities are modeled as O–C cavities. (The assumption

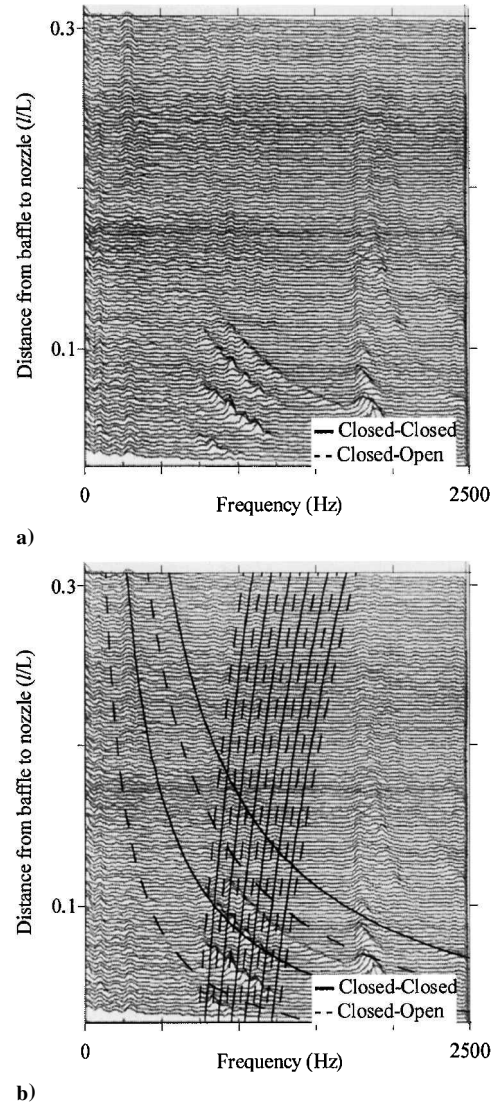

Fig. 10 Single-baffle study with a 5.8-cm-diam rigid baffle: a) pressure autospectra and b) spectra with superposition of frequencies of C–C and C–O acoustic modes formed between the baffle and the ends of the test section.

of different acoustic impedances at the upstream and downstream baffles was cited as a point of concern by one reviewer. Although the authors are not familiar with prior work that would justify this claim, the assumption does fit the experimental data for two baffles. As discussed later, this was not true for a single baffle.)

For each of the 320 autospectra in the Fig. 2a, the maximum SPL and the frequency at which it occurred were identified. These are shown in Fig. 4a as discrete data plotted against the distance between the downstream baffle and the nozzle. Figure 4a also shows curves depicting the resonant frequencies of the baffle-to-nozzle and baffle-to-inlet cavities as they vary with baffle position, as well as lines corresponding to (constant) inlet-to-nozzle chamber-length resonant frequencies. Figure 4b shows similar data for each spectral measurement in Fig. 2b. The fundamental baffle-to-baffle cavity resonance occurs at 1280 Hz for the data in Fig. 4a and 925 Hz in Fig. 4b, but, because they do not coincide with hole-tone frequencies, they are not shown.

Nine discrete bands of hole-tone frequencies are presented in Fig. 4a. Within each band, frequencies lock-in to the downstream baffle-to-nozzle cavity's resonant frequencies from roughly 900 to 840 Hz (the inlet-to-nozzle cavity's 10th mode) and below 840-Hz lock-in to the upstream baffle-to-nozzle cavity's resonant frequencies. More specifically, as the distance between the downstream baffle and the nozzle increases from 5 cm, hole-tone lock-in occurs due to the first downstream baffle-to-nozzle mode, then the 10th

inlet-to-nozzle mode, the first upstream baffle-to-nozzle mode, the second downstream baffle-to-nozzle mode, the 10th inlet-to-nozzle mode, the second upstream baffle-to-nozzle mode, the third downstream baffle-to-nozzle mode, etc.

Seven discrete bands of decreasing hole-tone frequencies are presented in Fig. 4b with lock-in jumping to different acoustic modes in a fashion similar to that seen in Fig. 4a. For this baffle spacing, lock-in tends to coincide with either the eighth inlet-to-nozzle cavity resonance or one of the upstream baffle-to-nozzle cavity resonances. Hole-tone lock-in to resonance of the downstream baffle-to-nozzle cavity occurs only in two bands at the right of Fig. 4b, where the downstream and upstream baffle-to-nozzle resonances are quite close to one another. Between five of the bands, larger hole-tone responses are produced by stage-2 vortex shedding than by stage-1 vortex shedding (at 1050–1150 vs 600–700 Hz). This occurs when coincidence of the third downstream baffle-to-nozzle, the second upstream baffle-to-nozzle, and the 11th inlet-to-nozzle resonances occur, providing stage-2 vortex shedding reinforcement that is stronger than stage-1 vortex shedding reinforcement provided by eighth inlet-to-nozzle resonance.

The SPLs from the 6.5-cm baffle spacing results in Fig. 4a were generally 2–3 dB higher than the SPLs measured in the 9.0-cm baffle spacing results in Fig. 4b. This is in agreement with previous results and the explanation presented by Rockwell (Lehigh University) that the strength of feedback and instability reinforcement increases with a decreasing distance between where a vortex is shed and the downstream surface where dipole acoustic radiation occurs.

In both Figs. 4a and 4b, hole-tone SPLs decrease at the edges of each discrete frequency band. The range of SPLs within a given band show differences of up to 15 dB in Fig. 4a and up to 10 dB in Fig. 4b. The largest SPLs occurred when the hole-tone frequency coincided with the resonance of multiple acoustic cavities. In Fig. 4a, coincidence of the 10th inlet-to-nozzle mode with either an upstream or downstream baffle-to-nozzle mode produced the largest hole-tone SPLs. In Fig. 4b, coincidence of the eighth inlet-to-nozzle mode with either an upstream or downstream baffle-to-nozzle mode produced the largest SPLs.

In summary, Figs. 4a and 4b both indicate that the frequency of lock-in will coincide with the frequency of acoustic reinforcement that provides the strongest reinforcement near either the stage-1 or stage-2 nominal vortex shedding frequencies. Resonance of the upstream baffle-to-nozzle, downstream baffle-to-nozzle, and inlet-to-nozzle cavities appear to "compete" equally as reinforcement mechanisms. Coincidence of two of these resonances (typically an inlet-to-nozzle resonant frequency and either a downstream or upstream baffle-to-nozzle cavity resonant frequency) significantly amplifies the strength of the resultant hole tone.

Test Case 2: Varied Baffle-to-Baffle Spacing ($1.2 \leq d/B \leq 6.2$ and $l/L = 0.38$)

The effect of baffle spacing on the frequency and amplitude of hole-tone acoustic responses was studied by locating the upstream baffle 74.5 cm from the nozzle, for a dimensionless upstream baffle position of $l/L = 0.38$, and increasing the distance to the downstream baffle d from 7.0 to 36.0 cm in 0.5-cm increments. Rigid baffles with an inner diameter B of 5.8 cm were used for the results shown in Fig. 5, corresponding to varying the dimensionless baffle spacing d/B from 1.2 to 6.2. Autospectra with similar results from tests of four additional upstream baffle positions ($l/L = 0.40$–0.48) are presented in Ref. 35.

Responses at vortex shedding stages 1–4 (stage 1 at the lower left to stage 4 at the upper right) are shown as four separate lightly shaded ridges of peaks in the autospectra in Fig. 5a. Nominal Strouhal numbers of 0.9, 1.6, 2.5, and 3.5 corresponding to stages 1–4 vortex shedding were empirically determined from this test and over 30 similar tests.[35] These Strouhal numbers were determined using Eq. (1) with d as the interbaffle spacing and the mean instability velocity U as 67% of the free-field mean flow velocity past the upstream baffle as suggested by Rossiter.[32]

The largest hole-tone responses in Fig. 5a occur in four small groups of stage-1 and stage-2 acoustic peaks (enclosed by a circle). As the dimensionless baffle spacing increased from 1.2, hole-tone peaks were initially driven by stage-1 vortex shedding at ~700 Hz. At a spacing of $d/B = 1.9$, the largest responses were driven by stage-2 vortex shedding at ~900 Hz. At 2.1, the largest responses jumped back to being driven by stage-1 vortex shedding at ~450 Hz. Then, for a spacing of 2.4, they again jumped to being driven by stage-2 vortex shedding at ~750 Hz. As baffle-to-baffle spacing increased above 3.1, the amplitude of vortex shedding induced responses dropped off, and the pressure spectra generally resembled background acoustic responses.

The frequencies of peak SPL as a function of baffle spacing are plotted in Fig. 5b, along with curves corresponding to the frequencies predicted by Eq. (1), to reflect lines of constant Strouhal number bounding stage-1 and stage-2 vortex shedding. In addition, curves showing the frequencies of acoustic modes for the inlet-to-nozzle C–C acoustic cavity, the downstream baffle-to-nozzle O–C acoustic cavity, and the upstream baffle-to-nozzle C–C acoustic cavity based on Eqs. (3) and (4) are shown.

The area enclosed in the ellipse illustrates that, as the baffle spacing was increased from d/B of 1.2, hole tones were driven first by coincidence of baffle-to-nozzle mode-3 and stage-1 vortex shedding. Then, as mode-3 frequencies increased and diverged from nominal stage-1 vortex shedding frequencies, coincidence of baffle-to-nozzle mode-4 and stage-2 vortex shedding became the driving reinforcement mechanism for lock-in of the flow instability and hole-tone generation process. As mode-4 and stage-2 vortex shedding frequencies diverged, reinforcement due to lock-in of mode-1 and stage-1 vortex shedding drove the hole-tone generation process, and, on their divergence, coincidence of mode-3 with stage-2 vortex shedding drove the hole-tone generation process.

Experimental work on edge tones by Ziada and Rockwell[36] indicates that for the general case of vortex–edge interactions, vortex shedding frequencies occur at successively increasing stage numbers with increasing impingement length. Results in Fig. 5 indicate that acoustic reinforcement of vortex shedding can modify this trend.

For the baffle spacing range from $d/B = 3.2$–3.8, no hole tones were generated, and the peak SPLs were due to low-frequency background noise. In this baffle spacing range, the inlet-to-nozzle sixth-mode resonant frequency coincided with the stage-2 vortex shedding frequencies; however, resonance of the baffle-to-nozzle cavities did not. Insufficient instability reinforcement occurred to sustain hole-tone generation. As the baffle spacing increased beyond this range, however, coincidence of stage-2 and stage-1 vortex shedding with downstream, and then upstream, baffle-to-nozzle cavity resonance occurred, and hole tones were excited at baffle spacings out to $d/B = 4.7$. Beyond baffle spacings of 4.7, SPL levels were again at the background noise level with a response due to stage-1 vortex shedding at the second inlet-to-nozzle acoustic cavity mode, marginally above that of other frequencies.

Hole-tone reinforcement due to lock-in with resonance of a C–O acoustic cavity formed between the baffles was not observed. The baffle-to-baffle cavity resonant frequencies overlap the range of excited hole-tone frequencies, with a fundamental mode resonance decreasing from 925 to 595 Hz as baffle-to-baffle spacing increased from 9.0 to 14.0 cm. Resonance curves for this acoustic cavity are similar in shape to the vortex shedding frequency curves (both functions of $1/d$), but did not overlap with the vortex shedding bands or with hole-tone frequencies.

Test Case 3: Variable Baffle Diameter ($d = 5.3$, 5.8, and 6.3 cm; $1.2 \leq d/B \leq 6.2$; and $l/L = 0.43$)

Data sets were collected using three baffle inner diameters to obtain three different flow velocities past the baffles and, therefore, three different sets of nominal vortex shedding frequencies for a given baffle pair location in the test section. Figure 6 shows waterfall plots for 5.3-, 5.8-, and 6.3-cm inner diameter aluminum baffle data at similar locations in the test section.

For the three different flow velocities, trends similar to those already discussed are present, indicating vortex shedding frequency lock-in to the baffle-to-nozzle cavity modes. Also, jumping of the dominant acoustic response between stage-1 and stage-2 vortex

shedding is observed, with the best match between baffle-to-nozzle cavity resonance and the mean vortex shedding frequencies of the different stages appearing to drive the stage of vortex shedding that dominates the hole-tone acoustic response.

As expected, the amplitude of the acoustic responses increases as the baffle inner diameter decreases. The velocity of flow shed by the upstream baffle increases with decreasing baffle diameter, thereby increasing the strength of the shed flow instability and the resultant acoustic field. As in the second test case presented, no indication of lock-in associated with baffle-to-baffle cavity resonances is evident in the data.

Test Case 4: Varied Baffle Stiffness ($1.2 \leq d/B \leq 5.1$ and $l/L = 0.38$)

In addition to the rigid baffles used in test cases 1–3, data were also taken using rubber (soft) and two different thickness brass (stiff) baffles. Figures 7a–7d show acoustic pressure autospectra for pairs of 5.8-cm inner diameter soft, stiff, and rigid baffles with the upstream baffle position fixed at $l/L = 0.38$. The baffle spacing d/B was varied from 1.25 to 5.1. With only one exception, shown in Fig. 7e, variations in the stiffness of the baffles did not produce significant differences in the hole-tone responses shown in Figs. 7a–7d.

The only data set in which resonance of either baffle had a significant and reproducible effect on the hole-tone generation process occurred when the upstream baffle second-mode resonance coincided with the vortex shedding frequency and the 10th test-section acoustic mode at 840 Hz. Interestingly, it was the second baffle resonant mode, not the first, that triggered significant amplification of the hole tone. In contrast with a mode-1 baffle response, in which the baffle surface moves in phase, mode 2 has one nodal diametral line, with out-of-phase motion on opposite sides of this nodal diameter. This produced the shift in the dominant hole-tone frequency and significant amplification of the hole-tone SPL at d/B of 1.2, shown in the bottom waterfall plot of Fig. 7e for the 0.4-mm-thick brass baffle. In Figs. 7a–7c, the SPL of the peak at this position was between 143.5 and 146.0 dB, and, Fig. 7d the peak SPL was 158.4 (Ref. 35). Weak excitation of the chamber-length mode at 840 Hz was present in the other spectra measured for this baffle configuration (about 10 dB less than the 145-dB hole-tone response at 780 Hz). At 780 Hz, vortex shedding had locked in to the baffle–nozzle frequencies, not the chamber-length acoustic mode. The addition of the baffle structural resonance at the frequency of the chamber-length mode apparently modified the balance of energies sufficiently that the source of acoustic lock-in switched from the baffle-to-nozzle mode to the inlet-to-nozzle mode, with the quite significant SPL increase of over 12 dB. This resonant baffle response was reproduced using two different upstream baffles that were both instrumented with three strain gauges. The strain measurements verified the asymmetry of the baffle resonant motion at the hole-tone frequency.

Other test cases in which the upstream baffle second mode (based on resonance measured before tests) matched hole-tone frequencies for somewhat larger baffle-to-baffle spacing did not produce a noticeable change in the acoustic response. One explanation for this is that lock-in to a chamber-length mode allows resonant baffle motion to pump energy into the acoustic field more easily than lock-in to either baffle-to-nozzle acoustic field mode did alone. (The baffle-to-inlet spacing would introduce cancellation of energy unless spacing was such that a standing wave could also be introduced upstream of the baffles, which is the case of matching the test-section resonances.) Alternatively, perhaps the larger baffle-to-baffle spacing needed for frequency coincidence disrupted the precise phase relationship between the structural mode and acoustic reinforcement, or simply weakened the hole-tone reinforcement mechanisms, which made less energy available to excite the baffle resonance.

Figures 8a and 8b show normalized strain data for the baffles in Figs. 7a and 7b. For the aluminum baffles, no strains were detected with the instrumentation used. In all data sets the downstream baffles exhibited responses over a broader range of frequencies than the upstream baffles. Upstream baffles exhibited slightly larger strains at the hole-tone frequency than the downstream baffles. Also, not surprisingly, the soft baffles flexed more than the stiff baffles (larger magnitude of strains and larger bandwidth of response). Over a significant portion of the bandwidth, at frequencies other than near the vortex-shedding frequencies, the strain response was too small to be detected, especially for the stiff baffles. Harmonics of low-level 60-Hz noise were of the same order of magnitude as the stiff baffle strain responses.

Figure 9a shows the frequencies of peak response, bands of stage-1 and stage-2 vortex shedding frequencies, and frequencies of acoustic cavity resonances. Figure 9b shows the SPLs measured at those peak frequencies. Although more variability is present in the hole-tone peak amplitudes than in the hole-tone frequencies, no clear trends related to the different baffle materials are evident. In general, the flexibility of these baffles has little or no effect on either hole-tone peak frequencies or amplitudes.

A detailed investigation of the interaction of structural resonances with vortex shedding was not conducted; however, some interesting preliminary observations related to structural resonance interaction with vortex shedding frequency lock-in will be summarized. Note, however, that baffle resonant frequencies before and after removal from the test section often showed changes (reductions) of up to 10% (Ref. 35). This made it difficult to assess accurately whether or not exact coincidence of the baffle resonance and the vortex shedding frequency had occurred while being tested.

In several data sets, when a downstream baffle's structural resonant frequencies should have coincided with that of the vortex shedding and hole tones, the downstream baffle appeared to behave like a tuned vibration absorber, causing a slight reduction in the hole-tone acoustic amplitude. Although this effect was not observed in all cases, as discussed earlier, baffle resonant frequencies shifted during test, which introduced uncertainty into knowing when baffle resonance and hole-tone coincidence actually occurred. As shown in Fig. 7e, coincidence of the upstream baffle second mode with the chamber-length acoustic mode introduced both a shift in frequency of vortex shedding lock-in and a significant increase in the amplitude of the hole tone. Further study, with the ability to check baffle resonance in situ, would aid in understanding this effect. These preliminary observations are presented for consideration and to motivate further study of these structural-flow interactions.

Test Case 5: Single-Baffle Tests ($0.9 \leq d/B \leq 10.5$ and $0.02 \leq l/L \leq 0.31$)

The position of a single baffle in the test section was varied to study the hole-tones produced by interaction of a single baffle and the downstream end of the test section. Data were obtained by moving a single rigid 5.8-cm inner diameter baffle in 0.5-cm increments from the nozzle end of the test section toward the inlet, for baffle positions l/L ranging from 0.02 to 0.31. These results are presented in Fig. 10. Stages 1–4 vortex shedding driven hole-tone responses are observed. Self-sustaining hole-tone generation occurred for a range of dimensionless baffle–nozzle spacing d/B of 0.9–3.3. Vortex shedding of flow past the microphone located near the inlet is evident as the low-level constant frequency response at approximately 1800 Hz (based on a Strouhal number of 0.2 for flow past a cylinder).[29] The largest acoustic responses occur when stages 2–4 vortex shedding between the baffle and nozzle coincide with this upstream 1800-Hz disturbance. In Fig. 10b, it is apparent that resonance of the baffle-to-nozzle acoustic cavity does not appear to drive vortex shedding frequency lock-in in this circumstance. For this geometry, the frequencies of C–C and C–O baffle-to-nozzle modes do not coincide with the bands of stage-1 or 2 vortex shedding based on the baffle-to-nozzle distance d. The second C–C baffle-to-nozzle mode does overlap the band of stage-3 vortex shedding, as shown in Fig. 10b, but this does not introduce noticeable amplification of the resultant hole tones. Rather, there is a stronger correlation to the hole-tone peaks at 800–1200 Hz and the baffle-to-inlet cavity O–C resonant frequencies. This matches the observations made about the region of $l/L < 0.3$ in Figs. 3a and 3b, where baffle-to-nozzle modes did not coincide with frequencies in the bands of stage-1 and stage-2 vortex shedding frequencies, but baffle-to-inlet modes did. Hence, they appeared to drive lock-in. In the two-baffle cases, the upstream and downstream baffles appeared to introduce different acoustic impedances with maximum SPL amplification occurring

when the baffles are one-quarter wavelength apart and at pressure antinodes and nodes, respectively, of one of the cavity's axial acoustic modes. This suggests that the upstream baffle behaves as a closed acoustic boundary. With only one baffle in the chamber, the baffle appears to act as a pressure release or open acoustic boundary. It is coincidence of the bands of stages 1–4 vortex shedding with the O–C baffle-to-inlet acoustic modes, not C–C modes, that introduces the observed hole-tone peaks.

Summary Discussion of Test Case Observation Relevance to Segmented Rocket Motors

The experimental work presented suggests that acoustic waves reflected at the downstream end of the test section have an equally strong potential to influence the hole-tone and vortex shedding mechanisms by influencing instability strength at the upstream baffle or by influencing dipole radiation strength at the downstream baffle. These influences will be maximized for an even number of one-quarter wavelengths between the upstream baffle and nozzle and for an odd number of one-quarter wavelengths between the downstream baffle and nozzle. The effect of these reinforcement mechanisms on SPL magnitudes was amplified when chamber-length acoustic mode frequencies coincided with these baffle-to-nozzle modes in a fashion that placed the upstream baffle at a chamber-length mode's pressure antinode or the downstream baffle at a chamber-length mode's pressure node.

In summary, when an odd number of one-quarter wavelengths fit between the two baffles and between the downstream baffle and nozzle, both flow instability strength at the upstream baffle and dipole radiation strength at the downstream baffle are reinforced. This baffle spacing occurs in solid-rocket motors fabricated from segments of similar lengths, whether the motor consists of an odd or even number of segments. An additional source of hole-tone generation and reinforcement in motors fabricated from an even number of equal-length motor segments is the potential for the additional coincidence with excitation of even chamber-length modes, which will produce pressure nodes and antinodes at segment interface locations. Segmented motors fabricated from N ($N > 2$) segments of the same length will exhibit strong reinforcement of the $N/2$ acoustic mode of the chamber. (That is, solid-rocket motors fabricated from four equal-length motor segments will exhibit strong vortex shedding reinforcement of the chamber-length mode-2 frequency, from six equal-length segments, strong mode-3 responses, etc.) Acoustic reinforcement should be lower in motors fabricated of an odd number of segments for which motor length acoustic standing wave pressure nodes and antinodes will not be coincident with segment interface locations. Use of segments of lengths that would interfere with these reinforcement mechanisms should further reduce hole-tone responses.

Conclusions

The data presented provide experimental evidence of factors influencing the vortex shedding lock-in process and amplification of the generated hole tones for flow through an approximately C–C cylindrical duct containing two annular baffles. The upstream baffle from which vortices are shed was accurately modeled as having high acoustic impedance. The downstream baffle upon which the vortices impinge was accurately modeled as having low acoustic impedance. The frequency of vortex shedding lock-in generally matches resonant frequencies of one of the two cavities formed by the baffles and the downstream end of the test section, namely, whichever of these two cavity resonances is closer to a nominal vortex shedding frequency. The maximum amplitude of the acoustic response was typically observed when either the upstream or the downstream baffle position coincided with standing wave antinodes and nodes, respectively, of the acoustic pressure standing waves formed in the cavity between the inlet and the nozzle.

One source of lock-in was the acoustic standing waves excited between the upstream baffle and the nozzle (a C–C cavity), which appears to cause lock-in by producing periodic reinforcement of flow instabilities at the upstream baffle. Another source of lock-in was the acoustic standing waves excited between the downstream baffle and the nozzle (an O–C cavity) which appear to cause lock-in by producing periodic reinforcement of acoustic radiation from the downstream baffle. Resonance of the inlet-to-nozzle cavity appears to cause frequency lock-in when these other two mechanisms are not present; however, this reinforcement mechanism produced lower hole-tone amplification, that is, lower SPLs, than the baffle-to-nozzle reinforcement mechanisms did.

Stages 1–4 Strouhal numbers of 0.9, 1.6, 2.5, and 3.5 were empirically determined for hole-tone generation in the range of Reynolds and Mach numbers studied. These Strouhal numbers remained fairly constant for nondimensional baffle spacings from 1.1 to ~5.0, above which negligible levels of hole-tone generation were detected.

Hole-tone acoustic response amplitudes and frequencies were found to be insensitive to baffle material, although significantly different levels of transverse bending motion were observed in tests with soft, stiff, and rigid baffles. The downstream baffles exhibited motion over a broader band of frequencies than the upstream baffles, whereas the upstream baffles underwent larger strains at the hole-tone frequencies than the downstream baffles.

For only one of the geometric configurations tested did structural resonance of a baffle change the interaction of the flowfield and acoustic field. Specifically, coincidence of the mode-2 upstream baffle bending resonance with the test-section mode-10 acoustic resonance contributed to a change in vortex shedding lock-in frequency and a significant (10-dB) amplification of the dominant hole-tone SPL. Observations of the interaction of downstream baffle resonance with hole-tone responses were inconclusive.

Acknowledgments

This project was initiated in conjunction with a research effort at Thiokol Corporation and was sponsored by Thiokol Corporation. The authors wish to express thanks to Thiokol Corporation and Program Manager Donald Mason, in particular, for their generous support throughout the progress of this project, to G. A. Flandro for his thoughts on initiating this research, and to Thomas Toby Hansen for his painstaking assistance in obtaining many of the extensive measurement sets used in this investigation. The material for the soft baffles was provided by F. Kelly from the University of Arkon's Polymer Sciences Laboratory.

References

[1]Culick, F. E. C., "Stability of Longitudinal Oscillations with Pressure and Velocity Coupling in a Solid Propellant Rocket," *Combustion and Science Technology*, Vol. 2, No. 4, 1970, pp. 179–201.

[2]Flandro, G. A., and Jacobs, H. R., "Vortex Generated Sound in Cavities," *Aeroacoustics: Jet and Combustion Noise, Progress in Astronautics and Aeronautics*, Vol. 37, MIT Press, Cambridge, MA, 1975, pp. 521–533.

[3]Culick, F. E. C., and Magiawala, K., "Excitation of Acoustic Modes in a Chamber by Vortex Shedding," *Journal of Sound and Vibration*, Vol. 64, No. 3, 1979, pp. 455–457.

[4]Culick, F. E. C., *Combustion Instability in Solid Rocket Motors—Volume II—A Guide for Motor Designers*, JANNAF Combustion Subcommittee, Motor Design Panel, Chemical Propulsion Information Agency, Publ. 290, 1980.

[5]Brown, R. S., Dunlap, R., Young, S. W., and Waugh, R. C., "Vortex Shedding as a Source of Acoustic Energy in Segmented Solid Rockets," *Journal of Spacecraft*, Vol. 18, No. 4, 1981, pp. 312–319.

[6]Dunlap, R., and Brown, R. S., "Exploratory Experiments on Acoustic Oscillation Driven by Periodic Vortex Shedding," *AIAA Journal*, Vol. 19, No. 3, 1981, pp. 408–409.

[7]Flandro, G. A., "Time Dependent Flows in Solid Propellant Rockets," Progress Rept. to Thiokol Corp., Aug. 1984.

[8]Brown, R. S., Dunlap, R., Young, S. W., and Waugh, R. C., "Vortex Shedding Studies in a Simulated Coaxial Dump Combustor," *Journal of Propulsion*, Vol. 1, No. 5, 1985, pp. 413–415.

[9]Shu, P. H., Sforzini, R. H., and Foster, W. A., Jr., "Vortex Shedding from Solid Rocket Propellant Inhibitors," AIAA Paper 86-1418, June 1986.

[10]Flandro, G. A., "Vortex Driving Mechanism in Oscillatory Rocket Flows," *Journal of Propulsion and Power*, Vol. 2, No. 3, 1986, pp. 206–214.

[11]Culick, F. E. C., "Combustion Instabilities in Liquid-Fueled Propulsion Systems—An Overview," CP 450, AGARD, Specialized Printing Services, Essex, England, U.K., 1989.

[12]Vuillot, F., Trainau, J. C., Prevost, M., and Lupoglazoff, N., "Experimental Validation of Stability Assessment Methods for Segmented Solid Propellant Motors," AIAA Paper 93-1883, June 1993.

[13]Scippa, S., Pascal, P., and Zanier, F., "Ariane-5 MPS: Chamber Pressure Oscillations Full Scale Firings Results Analysis and Further Studies," AIAA Paper 94-3068, June 1994.

[14]Vuillot, F., "Vortex-Shedding Phenomena in Solid Rocket Motors," *Journal of Propulsion and Power*, Vol. 11, No. 4, 1995, pp. 626–639.

[15]Prevost, M., Vuillot, F., and Traineau, J. C., "Vortex-Shedding Driven Oscillations in Subscale Mortors for the Ariane 5 MPS Solid Rocket Motors," AIAA Paper 96-3247, July 1996.

[16]Dotson, K. W., Koshigoe, S., and Pace, K. K., "Vortex Shedding in a Large Solid-Rocket Motor Without Inhibitors at the Segment Interfaces," *Journal of Propulsion and Power*, Vol. 13, No. 2, 1997, pp. 197–206.

[17]Anthoine, J., and Olivari, D., "Cold-Flow Simulation of Vortex Induced Oscillations in a Model of Solid Propellant Boosters," AIAA Paper 99-1826, May 1999.

[18]Stubos, A. K., Benocci, C., Pallo, E., Stoubos, G. K., and Olivari, D., "Aerodynamically Generated Acoustic Resonance in a Pipe with Annular Flow Restrictors," *Journal of Fluids and Structures*, Vol. 13, No. 6, 1999, pp. 755–778.

[19]Lupoglazoff, N., and Vuillot, F., "Numerical Simulation of Vortex Shedding Phenomenon in 2D Test Case Solid Rocket Motors," AIAA Paper 92-0776, Jan. 1992.

[20]Lupoglazoff, N., and Vuillot, F., "Parietal Vortex Shedding as a Cause of Instability for Long Solid Propellant Motors—Numerical Simulations and Comparisons with Firing Tests," AIAA Paper 96-0761, Jan. 1996.

[21]Couton, D., Doan-Kim, S., and Vuillot, F., "Numerical Simulation of Vortex-Shedding Phenomenon in a Channel with Flow Induced Through Porous Wall," *International Journal of Heat and Fluid Flow*, Vol. 18, No. 3, 1997, pp. 283–296.

[22]Lupoglazoff, N., and Vuillot, F., "Numerical Simulation of Parietal Vortex-Shedding Phenomenon in a Cold Glow Set-Up," AIAA Paper 98-3220, July 1998.

[23]Ugurtas, B., Avalon, G., Lupoglazoff, N., and Vuillot, F., "Numerical Computations of Hydrodynamic Instabilities Inside Channels with Wall Injection," AIAA Paper 99-2505, June 1999.

[24]Couton, D., Plourde, F., and Doan-Kim, S., Analysis of Energy Transfers of a Sheared Flow Generated by Wall Injection," *Experiments in Fliuds*, Vol. 26, No. 3, 1999, pp. 222–232.

[25]Avalon, G., Ugurtas, B., Grisch, F., and Bresson, A., "Numerical Computations and Visualization Tests of the Flow Inside a Cold Gas Simulation with Characterization of a Parietal Vortex Shedding," AIAA Paper 2000-3387, July 2000.

[26]Yildoz, D., Anthoine, J., and Buchlin, J. M., "Influence of Radial Injected Flow on the Aeroaoustic Coupling in Solid Propellant Boosters," AIAA Paper 2001-2101, May 2001.

[27]Rayleigh, J. W. S., The Theory of Sound, Dover, New York, Vol. 2, 1945, pp. 376–414.

[28]Chanaud, R. C., and Powell, A., "Some Experiments Concerning the Hole and Ring Tone," *Journal of the Acoustical Society of America*, Vol. 37, No. 5, 1965, pp. 902–911.

[29]Blake, W. K., *Mechanics of Flow-Induced Sound and Vibration*, Academic Press Inc., Orlando, Florida, 1986.

[30]Powell, A., "Theory of Vortex Sound," *The Journal of the Acoustical Society of America*, Vol. 36, No. 1, 1964, pp. 177–195.

[31]Blevins, R. D., "Review of Sound Induced by Vortex Shedding from Cylinders," *Journal of Sound and Vibration*, Vol. 92, No. 4, 1984, pp. 455–470.

[32]Rossiter, J. E., "Wind Tunnel Experiments on the Flow over Rectangular Cavities at Subsonic and Transonic Speeds," *Aeronautical Research Council, Ministry of Aviation*, Reports and Memoranda 3438, London, 1964.

[33]Nomoto, H., and Culick, E. C., "An Experimental Investigation of Pure Tone Generation by Vortex Shedding in a Duct," *Journal of Sound and Vibration*, Vol. 84, 1982, pp. 247–252.

[34]Umeda, Y., Maeda, H., and Ishii, R., "Hole Tone Generated from Almost Choked to Highly Choked Jets," *AIAA Journal*, Vol. 26, No. 9, 1988, pp. 1036–1043.

[35]Flatau, A. B., "Vortex Driven Sound in a Cylindrical Cavity," Ph.D. dissertation, Univ. of Utah, 1990.

[36]Ziada, S., and Rockwell, D., "Oscillations of an Unstable Mixing Layer Impinging Upon an Edge," *Journal of Fluid Mechanics*, Vol. 124, 1982, pp. 307–334.